Journal of Zhejiang University-SCIENCE A (Applied Physics & Engineering)
ISSN 1673-565X (Print); ISSN 1862-1775 (Online)
www.zju.edu.cn/jzus; www.springerlink.com
E-mail: jzus@zju.edu.cn

Experimental and numerical prediction of railway induced vibration

Hans VERBRAKEN†, Geert LOMBAERT, Geert DEGRANDE
(*Department of Civil Engineering, KU Leuven, Kasteelpark Arenberg 40 B2448, 3001 Heverlee, Belgium*)
†E-mail: hans.verbraken@bwk.kuleuven.be

Received Sept. 27, 2012; Revision accepted Oct. 12, 2012; Crosschecked Sept. 27, 2012

Abstract: In this paper, both measurements and numerical simulations of railway induced vibration are discussed. A measurement campaign has been carried out along the high-speed railway track in Lincent, Belgium. The experimental determination of transfer functions and vibration velocity during train passages are discussed. A numerical model is introduced to predict the transfer functions and the vibration velocity during train passages. The comparison of experimental and numerical results demonstrates the importance of accurate numerical models and input data. The results are obtained in the framework of the development of a hybrid prediction method, where numerical and experimental data can be combined to improve the prediction accuracy for railway induced vibration.

Key words: Component, Railway induced vibration, Experimental prediction, Numerical prediction
doi:10.1631/jzus.A12ISGT8 **Document code:** A **CLC number:** O32; TB53

1 Introduction

The development of the high-speed train network in Europe, the USA and Asia has led to increased attention for environmental vibrations due to railway traffic. An accurate prediction of ground vibration is required so that effective mitigation measures can be taken during the design process.

Several numerical models have been developed for the prediction of ground vibration due to railway traffic (Andersen and Jones, 2006; Lombaert *et al.*, 2006; Galvín and Dominguez, 2007). The advantage of numerical models is their flexibility in modeling a great variety of problems. An accurate estimation of the vibration requires accurate numerical models and input data, such as the dynamic track and soil characteristics, for which in situ testing may be required. A discrepancy is therefore often observed between numerical predictions and experimental results.

This paper discusses the results of a measurement campaign that has been carried out along the high-speed railway line between Brussels and Köln in Lincent, Belgium. Accelerometers have been installed on the track and in the free field. The transfer functions between the track and the free field have been determined by means of a hammer impact at several points along the railway track. This facilitates the determination of the transfer due to a line source on the track, which can be used to represent a train. Furthermore, the same measurement setup has been used to record the response during 103 train passages of different train types operating on the high-speed track.

In this paper, the experimental results obtained at the site in Lincent are discussed. Next, a numerical model based on the longitudinal invariance of the track is presented, which is used to predict the transfer functions and the vibration due to train passages. The predictions are compared to the experimental results.

The discrepancy between numerical and experimental results, due to insufficiently accurate models and input data, is investigated. As input data for numerical predictions are often extracted from experimental data such as transfer functions, the problem of input data accuracy can be partially avoided by directly using experimental transfer functions in the prediction. The research presented in this

paper is aimed at the development of such a hybrid prediction technique.

The paper is organized as follows. The measurement site in Lincent is presented in Section 2. In Section 3, the experimental results for the transfer functions and the vibration velocity during train passages are discussed. The numerical prediction model is introduced in Section 4 and used to predict the transfer functions and the vibration velocity. The numerical results are validated by means of the experimental results. The conclusions are presented in Section 5.

2 Measurement site

The site in Lincent is located next to the high-speed line between Brussels and Köln and has been frequently studied in the context of railway induced vibration and wave propagation in the soil. Previous vibration measurements have been performed during homologation tests of the high-speed line (Kogut and Degrande, 2003), while measurements of the rail receptance have been used to identify the dynamic characteristics of the track (Lombaert *et al.*, 2006).

The high-speed line consists of two tracks, one track in the direction of Köln (track 1) and the other in the direction of Brussels (track 2). These classical ballasted tracks have continuously welded UIC 60 rails that are supported every 0.60 m by resilient studded rubber pads on a prestressed monoblock concrete sleeper. From the rail receptance measurements, a rail pad stiffness k_{rp}=153.4×10^6 N/m and damping c_{rp}=13.5×10^3 Ns/m are obtained (Lombaert *et al.*, 2006). The sleepers have a length l_{sl}=2.5 m, a width w_{sl}=0.235 m, a height h_{sl}=0.205 m (under the rail) and a mass m_{sl}=300 kg. The track is supported by a porphyry ballast layer with a thickness h_b=0.35 m and a density ρ_b=1700 kg/m^3. From the rail receptance measurements, a ballast stiffness k_b=920.7×10^6 N/m (per sleeper) and damping c_b=16.6×10^3 Ns/m are obtained (Lombaert *et al.*, 2006). Under the ballast, a limestone sub-ballast layer with a thickness of 0.60 m is present and the soil is improved over a depth of 1.0 m by means of lime.

A number of seismic analysis of surface waves (SASW) tests and seismic cone penetration tests (SCPTs) have been performed in order to determine the soil layering and the dynamic soil characteristics. The results of an SASW test performed in 2008 reveal the presence of two layers on top of a half space (Coulier *et al.*, 2011). Table 1 summarizes for each layer the depth h, the shear wave velocity C_s, the dilatational wave velocity C_p, the material damping ratios β_s and β_p in shear and dilatational deformation, and the density ρ.

Table 1 Dynamic soil characteristics for the site in Lincent, Belgium (Coulier *et al.*, 2011)

Layer	h (m)	C_s (m/s)	C_p (m/s)	β_s	β_p	ρ (kg/m^3)
1	1.4	128	286	0.044	0.044	1800
2	2.7	176	286	0.038	0.038	1800
3	∞	355	1667	0.037	0.037	1800

Different train types are operating on the high-speed line: two InterCity (IC) trains and the Thalys and InterCity Experimental (ICE) high-speed trains. Both IC trains are composed of the same locomotive and coach type but contain a different number of coaches. The IC-A train has 13 carriages and a total length of 335.91 m, while the IC-O train has 7 carriages and a total length of 177.51 m. The Thalys train has an articulated composition with 10 carriages and a total length of 200.18 m, while the ICE train consists of 8 coaches with a distributed engine and has a total length of 200.32 m.

More details about the dynamic characteristics of the track, the soil and the rolling stock can be found in a report describing the measurement campaign (Verbraken *et al.*, 2012a).

3 Experimental results

3.1 Experimental setup

In March 2011 and May 2012, experiments have been carried out along the high-speed line L2 between Brussels and Köln in Lincent, Belgium (Verbraken *et al.*, 2012a; 2012b). The transfer function between the track and the free field has been determined by applying an impact force on the track and measuring the response in the free field. Furthermore, the free field response during 103 train passages has been measured.

Fig. 1 gives an overview of the experimental setup. A right-handed Cartesian frame of reference is

chosen on the ground surface with the origin at the center of track 2. The *x*-axis is perpendicular to the railway track, the *y*-axis is along the longitudinal axis of track 2 in the direction of Köln and the *z*-axis is pointing vertically upwards.

The test site has been instrumented with accelerometers at several points on the track and in the free field. Five measurement lines A, B, C, D and E are installed perpendicular to the track (Fig. 1). On these measurement lines, sixteen sensors are installed measuring the vertical acceleration. Eight sensors are installed on measurement line C and two sensors on each remaining measurement line. During the measurement of the transfer functions, one additional channel is added for the measurement of the impact force.

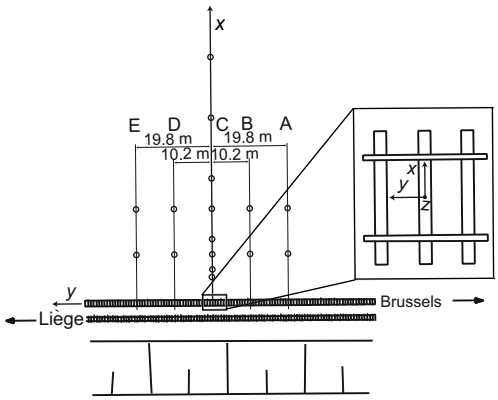

Fig. 1 Measurement setup at the site in Lincent

3.2 Transfer functions

For the determination of the transfer function between a source and a receiver point, a number of impacts are applied at the source point with an impact hammer recording the force, while the vertical acceleration is measured in the receiver point. The free field transfer function is determined from the impact on the edge of the sleeper as well as from the impact on the soil at 5.05 m from the center of track 2. In this study, only the transfer functions determined from the impact on the sleeper are discussed.

Several impact locations are selected along the track, so that the transfer due to a line load on the track can be determined. The impact points are denoted by the labels y*ii*, where the number *ii* refers to the *y*-coordinate of the impact point. Impact forces are applied on the track from $y=-100$ m to $y=100$ m with a spacing of 10 m.

In order to improve the signal-to-noise ratio of the experimental data, a large number of hammer impacts are recorded and the average transfer function is computed. The frequency content $\hat{f}_i^k(\omega)$ of the force at impact point *i* and the frequency content $\hat{v}_j^k(\omega)$ of the velocity in receiver *j* are determined for each impact *k*. The transfer function $\hat{H}_{ij}(\omega)$ between the impact point *i* and the receiver point *j* is then estimated by means of the H_1 estimator (Ewins, 1984):

$$\hat{H}_{ij}(\omega)=\frac{\hat{S}_{ji}(\omega)}{\hat{S}_{ii}(\omega)}. \tag{1}$$

The cross power spectral density $\hat{S}_{ij}(\omega)$ between channels *i* and *j* is computed as

$$\hat{S}_{ij}(\omega)=\frac{1}{N}\sum_{k=1}^{N}\hat{x}_i^k(\omega)\hat{x}_j^{k*}(\omega), \tag{2}$$

where $\hat{x}_i^k(\omega)$ is the frequency content of the signal in channel *i* for event *k*, $\hat{x}_j^{k*}(\omega)$ is the complex conjugate of $\hat{x}_j^k(\omega)$, and *N* is the total number of events. As each measurement leads to a different transfer function, the estimation $\hat{H}_{ij}(\omega)$ of the transfer function is a random variable for which a variance and a confidence interval can be computed. Fig. 2 shows the average transfer function and the 95% confidence interval obtained with 100 impacts on the track at impact point y00. At 6 m from the track (Fig. 2a), the transfer function is determined very accurately. The confidence interval is concentrated in a narrow region around the average value of the transfer function. At low frequencies, the uncertainty is slightly higher due to the low amplitude of the excitation. At 24 m from the track (Fig. 2b), the response is attenuated due to geometrical and material damping in the soil. As the higher frequencies correspond to a larger number of wavelengths over a certain distance, material damping results in a stronger attenuation of the amplitude in the higher frequency range. The signal-to-noise ratio decreases and the uncertainty of the transfer function increases with increasing distance from the track, especially in the higher frequency range.

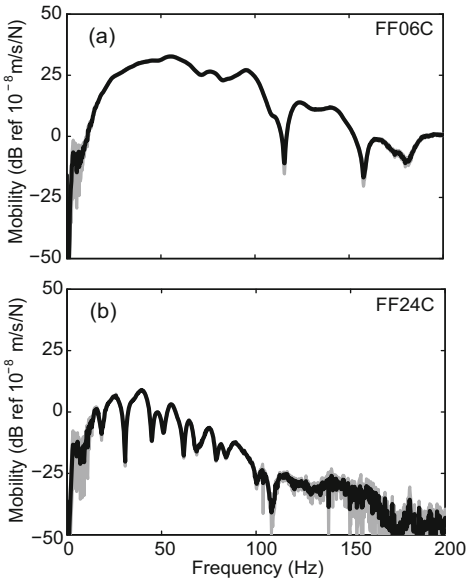

Fig. 2 Average mobility (black line) and 95% confidence interval (grey patch) determined with 100 impacts on the track at y00 at (a) 6 m and (b) 24 m from the track

Similar observations can be made for an impact point on the track at a larger distance from the measurement line. Fig. 3 shows the average transfer function and 95% confidence interval obtained with 100 impacts on the track at impact point y70. Due to the larger distance between the source and the receiver, the transfer function is smaller compared to the transfer function determined at y00 (Fig. 2), while the uncertainty increases.

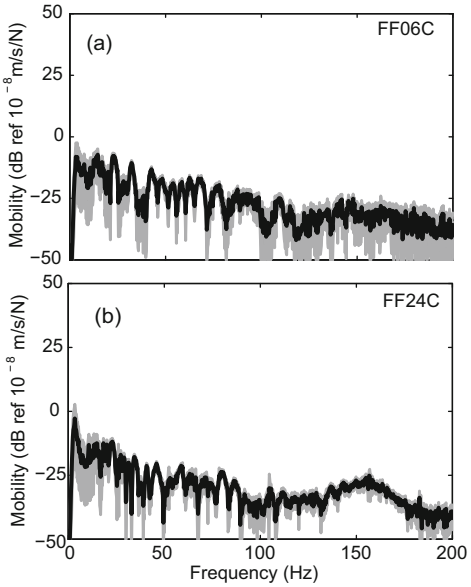

Fig. 3 Average mobility (black line) and 95% confidence interval (grey patch) determined with 100 impacts on the track at y70 at (a) 6 m and (b) 24 m from the track

The point transfer mobility TM_{Pk} $\left[\mathrm{dB\ ref}\ 10^{-8}\,\dfrac{\mathrm{m/s}}{\mathrm{N}}\right]$ is defined as the one-third octave band representation of the transfer function $\hat{H}_{ki}(\omega)$ between an impact point k and receiver point i (Hanson *et al.*, 2005; 2006):

$$\mathrm{TM}_{Pk}=10\log_{10}\left[\frac{\int_{\omega_1}^{\omega_2}|\hat{H}_{ki}(\omega)|^2\mathrm{d}\omega}{\Delta\omega}\right]-\mathrm{TM}_{P0}, \qquad (3)$$

where $\mathrm{TM}_{P0}=10\log10[10^{-8}]$ is the reference value of the point transfer mobility. The point transfer mobility TM_{Pk} is also a statistical variable for which a variance and a confidence interval can be computed.

Figs. 4 and 5 show the average point transfer mobility and 95% confidence interval determined with 100 impacts on the track at impact points y00 and y70, respectively. As the point transfer mobility is an averaged value in one-third octave bands, the uncertainty in a frequency band decreases compared to the narrow band transfer function, assuming independence at different frequencies. For both impact points y00 and y70, a relatively accurate estimate of the point transfer mobility is determined from the measurements, with a maximum confidence interval of 5 dB.

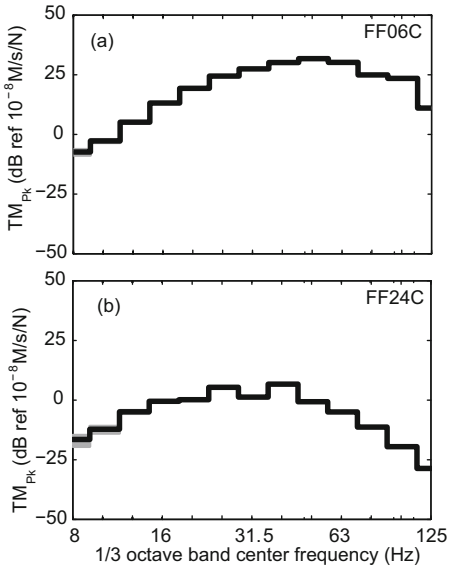

Fig. 4 Average point transfer mobility (black line) and 95% confidence interval (grey patch) determined with 100 impacts on the track at y00 at (a) 6 m and (b) 24 m from the track

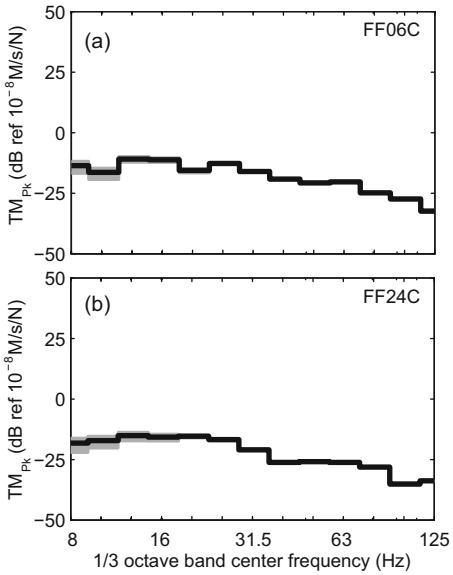

Fig. 5 Average point transfer mobility (black line) and 95% confidence interval (grey patch) determined with 100 impacts on the track at y70 at (a) 6 m and (b) 24 m from the track

The line transfer mobility $\mathrm{TM_L}$ $\left[\mathrm{dB\ ref}\,10^{-8}\,\dfrac{\mathrm{m/s}}{N/\sqrt{m}}\right]$ represents the vibration energy that is transmitted through the soil due to a line source and can be used to represent a train on the track. The line transfer mobility is determined based on the summation of n point transfer mobilities $\mathrm{TM}_{\mathrm{P}k}$ obtained from n impact points k along the track (Hanson *et al.*, 2005; 2006):

$$\mathrm{TM_L} = 10\log_{10}\left[h\sum_{k=1}^{n}10^{\frac{\mathrm{TM}_{\mathrm{P}k}}{10}}\right]. \qquad (4)$$

Fig. 6 shows the line transfer mobility obtained with a source length of 200 m and an impact point spacing of 10 m. Close to the track, the peak of the line transfer mobility is situated around 63 Hz. The line transfer mobility is attenuated with increasing distance from the track. As the attenuation in the soil is stronger for higher frequencies, this peak is shifted to lower frequencies.

3.3 Train passages

The free field response has been recorded during 103 train passages on both tracks. The following train passages with varying speeds have been measured on track 2 in the direction of Brussels: 30 IC-A passages (159 to 211 km/h), 10 IC-O passages (104 to 196 km/h), seven Thalys passages (156 to 293 km/h), and five ICE passages (214 to 242 km/h).

Fig. 7 shows a wiggle plot of the time history of the vertical velocity on measurement line C during the passage of an IC-A train and a Thalys train. The IC-A train has a length of 335.91 m and a speed of 198 km/h, corresponding to a duration of 6.11 s. The Thalys train has a length of 200.18 m and a speed of 281 km/h, corresponding to a duration of 2.56 s. Close to the track, the passage of individual axles can be distinguished. With increasing distance to the track, the contribution of an individual axle to the response becomes longer so that the duration of the response increases and the contribution of individual axles can no longer be distinguished.

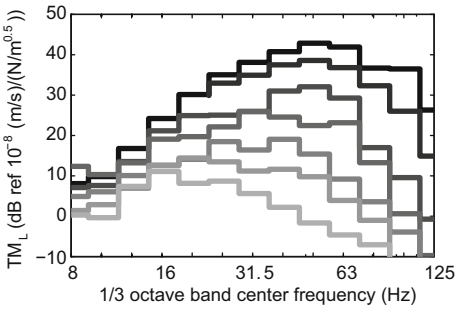

Fig. 6 Average line transfer mobility on measurement line C at 6 m to 64 m from the track (black to grey lines)

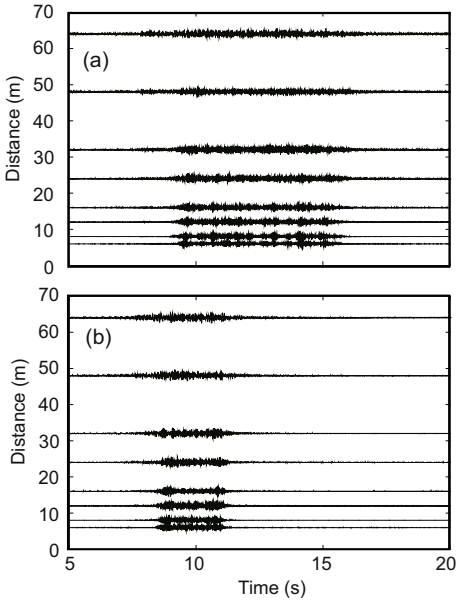

Fig. 7 Wiggle plot of the vertical velocity on measurement line C for (a) an IC-A passage at 198 km/h and (b) a Thalys passage at 281 km/h

The time history of the free field velocity is characterized by an increasing vibration level when the train approaches, an approximately stationary part during the pass-by, and a decreasing vibration level when the train is leaving. The vibration velocity L_V (dB ref 10^{-8} m/s) in the free field is defined as the one-third octave band root mean square (RMS) value of the stationary part.

Fig. 8 shows the vibration velocity during 30 passages of IC-A trains on track 2 in a speed range from 159 to 211 km/h, where a large variation is observed for different passages. This variation is due to differences in train speed and vehicle characteristics. The train speed is indicated in Fig. 8 with a different grey color, a darker color indicating a higher speed. An increased train speed might increase the vibration velocity, but also shifts the peak of the vibration velocity to a higher frequency. The effect of the train speed on the vibration velocity is therefore not clearly observed in these results.

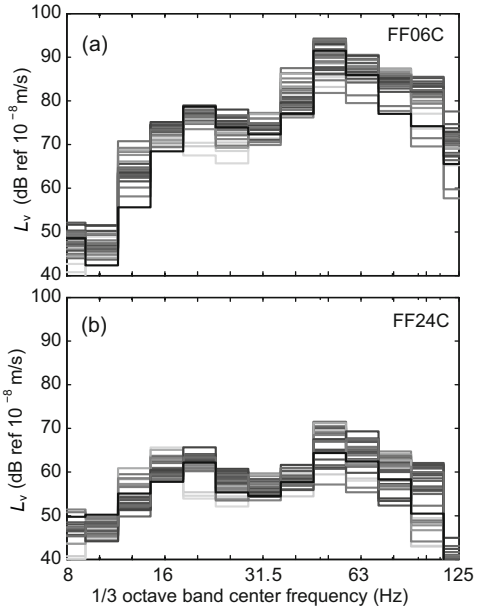

Fig. 8 Vibration velocity at (a) 6 m and (b) 24 m from the track during 30 passages of IC-A trains in a speed range from 159 to 211 km/h (grey to black lines)

A number of passages of IC-A trains in a narrow speed range are subsequently selected so that the effect of the train speed is eliminated. Fig. 9 shows the vibration velocity during nine passages of IC-A trains in a speed range from 193 to 197 km/h. The variation between different passages is smaller, especially in the frequency range between 10 and 31.5 Hz. A larger variation is still observed in the frequency range between 31.5 and 100 Hz. As the train speed does not vary much for the selected passages, this variation may be determined by differences in dynamic vehicle characteristics or wheel unevenness. The variation in the lower frequency range observed in Fig. 8 might be determined by the variation of the train speed.

In general, two peaks are observed in the vibration velocity during passages of IC-A trains (Figs. 8 and 9): a first peak is observed around 20 Hz while a second peak is observed around 50 Hz. These peaks are determined by the excitation (wheel and rail unevenness) and the dynamic characteristics of the vehicle and the track. Closer to the track, the response is dominated by the second peak. Due to material damping in the soil, however, the response is attenuated with increasing distance, especially for higher frequencies, and the second peak becomes less dominant at larger distances.

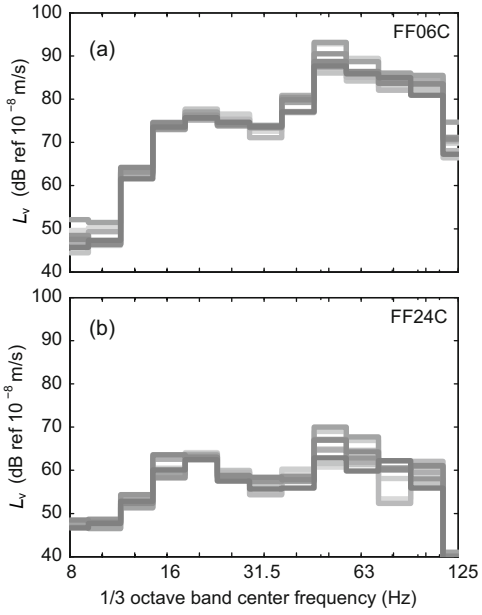

Fig. 9 Vibration velocity at (a) 6 m and (b) 24 m from the track during nine passages of IC-A trains in a speed range from 193 to 197 km/h (grey to black lines)

Fig. 10 shows the vibration velocity during five passages of Thalys trains on track 2 in a speed range from 281 to 293 km/h. A relatively small variation in the vibration velocity is observed. As the speed range is relatively small, this indicates that the variation of the vehicle characteristics and the wheel unevenness of the Thalys trains is relatively small.

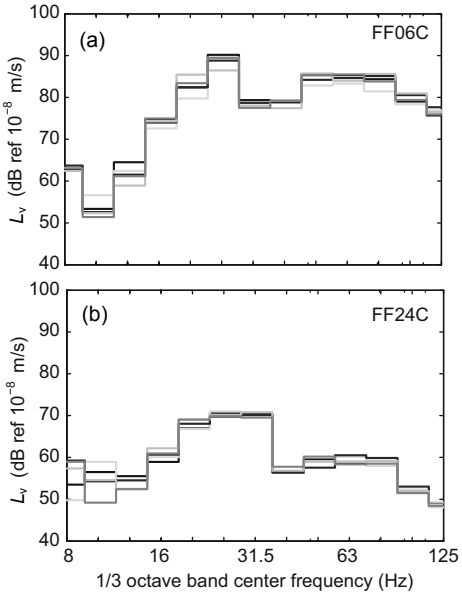

Fig. 10 Vibration velocity at (a) 6 m and (b) 24 m from the track during five passages of Thalys trains in a speed range from 281 to 293 km/h (grey to black lines)

Fig. 11 compares the average vibration velocity for each train type. As the previous results have shown that the vibration velocity is influenced by the train speed, the average value is computed for a number of passages within a relatively small speed range, where outliers have been removed. The average vibration velocity is computed for 25 IC-A passages (178 to 200 km/h), seven IC-O passages (192 to 196 km/h), five Thalys passages (281 to 293 km/h), and four ICE passages (238 to 242 km/h).

The IC trains result in a very similar vibration velocity level, as they are composed of the same type of carriages with only a different number of coaches. The first peak in the spectrum around 20–25 Hz is higher and more pronounced for the Thalys trains and also occurs at a higher frequency than for other train types with a lower train speed. The second peak around 50–63 Hz is lower for the Thalys and the ICE trains, which might be due to different dynamic vehicle characteristics of wheel unevenness. As the second peak is attenuated stronger with increasing distance from the track, the highest response at larger distances is obtained for the Thalys and ICE trains.

The global vibration velocity level $L_{\mathrm{v}}^{\mathrm{global}}$ represents the total vibration energy in all frequency bands and can be computed as

$$L_{\mathrm{v}}^{\mathrm{global}} = 10\log_{10}\left[\sum_i 10^{L_{\mathrm{v}}^i/10}\right], \tag{5}$$

where L_{v}^i represents the vibration velocity in the ith one-third octave band.

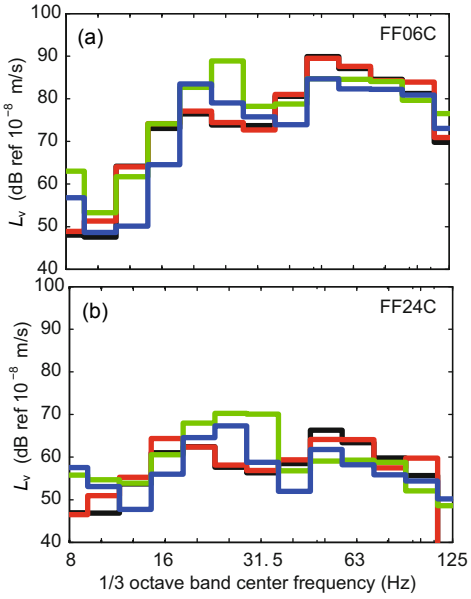

Fig. 11 Comparison of the average vibration velocity due to an IC-A (black line), IC-O (red line), Thalys (green line) and ICE (blue line) train at (a) 6 m and (b) 24 m from the track
Note: for interpretation of the references to color in this figure legend, the reader is referred to the web version of this article

Fig. 12 shows the global vibration velocity level $L_{\mathrm{v}}^{\mathrm{global}}$ averaged for each train type (in a limited speed range) as a function of the distance from the track. Close to the track, the vibration level of the IC trains is higher due to the dominant second peak around 50–63 Hz, which is less pronounced for the Thalys and the ICE trains. Due to material damping in the soil, this peak at higher frequencies is attenuated stronger with increasing distance. As the first peak around 20–25 Hz is slightly higher for the Thalys and ICE trains, the highest global vibration velocity level at large distance is found for these train types.

Fig. 13 shows the global vibration velocity level for each individual passage on track 2 as a function of the train speed at 6 m and 24 m from the track. The effect of the train speed on the vibration velocity level is relatively small. The variation of vibration velocity levels is higher for the IC trains, especially close to the track, and decreases with increasing distance from the track. These variations are observed in a relatively

narrow speed range and are therefore not due to differences in train speed.

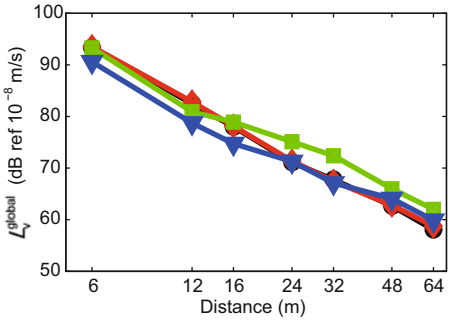

Fig. 12 Global average vibration velocity level in function of the distance for an IC-A (black circles), IC-O (red diamonds), Thalys (green squares) and ICE (blue triangles) train

Note: for interpretation of the references to color in this figure legend, the reader is referred to the web version of this article

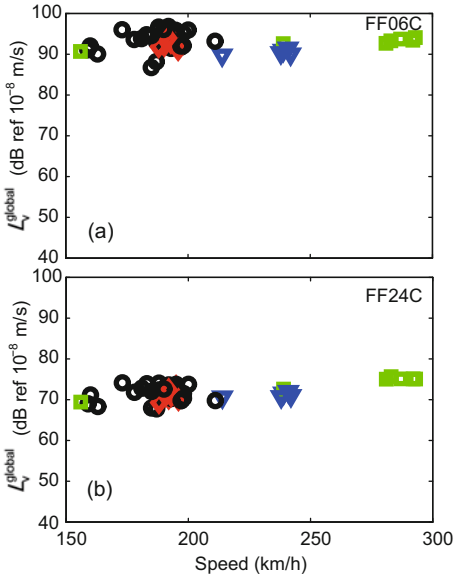

Fig. 13 Global vibration velocity level in function of the train speed for IC-A (black circles), IC-O (red diamonds), Thalys (green squares) and ICE (blue triangles) trains at (a) 6 m and (b) 24 m from the track

Note: for interpretation of the references to color in this figure legend, the reader is referred to the web version of this article

4 Numerical results

4.1 Numerical model

In this section, a numerical model of the track and the soil is used to simulate the line transfer mobility numerically.

The track-soil system is modeled by means of a coupled 2.5D finite element-boundary element (FE-BE) model (Lombaert *et al.*, 2006; François *et al.*, 2010) (Fig. 14). An efficient formulation is obtained by means of a double forward Fourier transform from the time domain to the frequency domain and from the spatial domain to the wavenumber domain. The track and the soil are assumed to be invariant in the longitudinal direction y. Fig. 14 shows the cross section of the model. The rails are modeled as Euler-Bernoulli beams, the rail pads as continuous spring-damper connections and the sleepers as a uniformly distributed mass, rigid in the plane of the cross section. The sleepers are supported by a ballast layer, which is modeled as an elastic continuum with 2.5D finite volume elements. The soil is modeled by means of 2.5D boundary elements at the interface between the ballast and the soil.

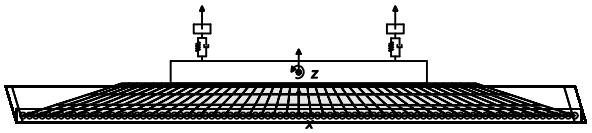

Fig. 14 Cross section of the track and soil model

The dynamic characteristics of the track and the soil, discussed in Section 3, are used for the computation of the transfer functions. However, as the characteristics of the ballast layer have been fitted to experimental results by means of a different numerical model, alternative ballast properties are considered based on practical tests (Coulier *et al.*, 2011). The ballast is modeled as an isotropic elastic continuum with a density ρ=1700 kg/m, a Young's modulus E=408×10^6 N/m^2 and a Poisson's coefficient ν=1/3. With these data, a ballast stiffness k_b=684.7×10^6 N/m is obtained.

As the presence of the second track can be disregarded when computing the transfer functions, only the ballast under track 2 is modeled with a trapezoidal shape with a top width w_{top}=3.6 m and a bottom width w_{bottom}=5.6 m (Fig. 14).

4.2 Transfer functions

Fig. 15 shows the predicted free field transfer function $\hat{H}(y,\omega)$ for an impact at point y00, compared to the experimental transfer function. Fig. 16 shows the transfer function determined with impacts at point y70. Close to the track (Fig. 15) the

experimental result is approximated relatively well by the predicted transfer function, while at larger distance (Fig. 16) the experimental transfer function is underestimated.

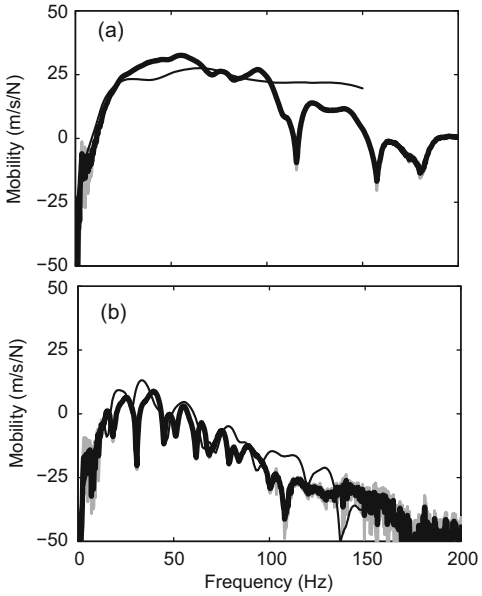

Fig. 15 Average experimental mobility (thick line) and 95% confidence interval (grey patch) and predicted mobility (thin line) for impacts on the track at point y00 at (a) 6 m and (b) 24 m from the track

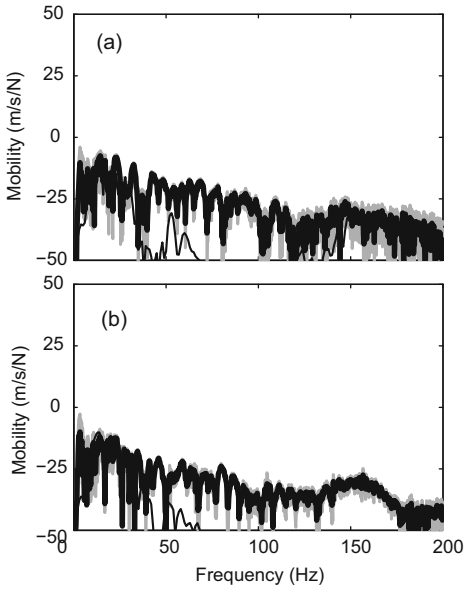

Fig. 16 Average experimental mobility (thick line) and 95% confidence interval (grey patch) and predicted mobility (thin line) for impacts on the track at point y70 at (a) 6 m and (b) 24 m from the track

Figs. 17 and 18 show the point transfer mobilities at the same impact points and lead to similar observations. While the point transfer mobility is predicted relatively well for a short source-receiver distance (Fig. 17), it is overestimated in the low frequency range and underestimated in the high frequency range for a larger source-receiver distance

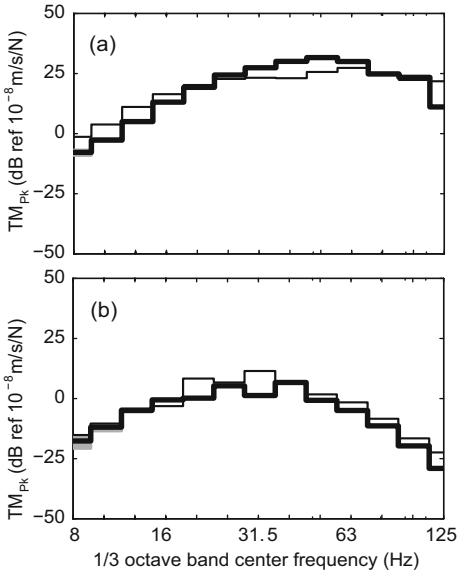

Fig. 17 Average experimental point transfer mobility (thick line) and 95% confidence interval (grey patch) and predicted point transfer mobility (thin line) for impacts on the track at point y00 at (a) 6 m and (b) 24 m from the track

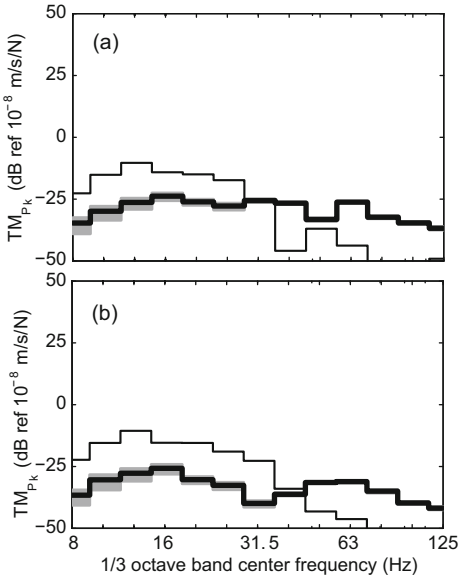

Fig. 18 Average experimental point transfer mobility (thick line) and 95% confidence interval (grey patch) and predicted point transfer mobility (thin line) for impacts on the track at point y70 at (a) 6 m and (b) 24 m from the track

(Fig. 18). The difference between the experimental and the predicted transfer function is caused by a discrepancy in the numerical model or in the dynamic characteristics.

Fig. 19 shows the predicted line transfer mobility obtained with a source length of 200 m and an impact point spacing of 10 m, at 6 m to 64 m from the track. When the predicted line transfer mobility in Fig. 19 is compared to the experimental result in Fig. 6, a relatively good agreement is found. Also the effect of the attenuation in the soil is predicted relatively well. A discrepancy up to 10 dB is found, but the agreement between the predicted and experimental results is better than those for the point transfer mobilities. This can be explained by the fact that the point transfer mobilities close to the measurement point, which are more accurate, contribute more to the line transfer mobility than the point transfer mobilities at larger distance. The discrepancy in the line transfer mobility is therefore limited.

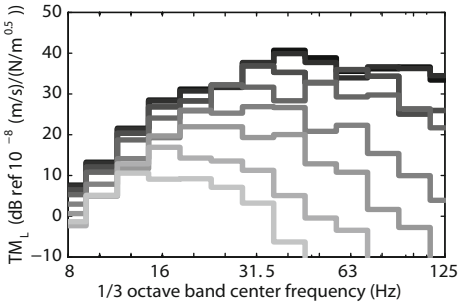

Fig. 19 Average predicted line transfer mobility at 6 to 64 m from the track (black to grey lines)

The observed discrepancy between the predicted and the experimental results shows the importance of accurate numerical models and input data. Input data for numerical predictions are often extracted from experimental results such as measured transfer functions, and are not always easy to determine accurately. This problem is partially avoided when measured transfer functions are directly used in predictions. It is important to note that experimental transfer functions can be combined with predicted input data for the source such as dynamic axle loads during a train pass-by and results in a hybrid prediction technique.

4.3 Train passages

For long trains with a speed well below the wave velocities in the soil, the stationary vibration velocity can be estimated by assuming the position of the moving axle loads to be fixed. The vibration velocity is then predicted based on the track-free field transfer function $\hat{H}(y,\omega)$ and the vertical axle loads $\hat{S}_{g_z kk}(\omega)$ of each axle k (Verbraken *et al.*, 2011):

$$L_{\mathrm{v}} = 10\log_{10}\left[\int_{\omega_1}^{\omega_2} |\hat{H}(y-y_k,\omega)|^2\, \hat{S}_{g_z kk}(\omega)\mathrm{d}\omega\right], \quad (6)$$

where y_k represents the position of the kth axle. The unevenness of the rail, measured at the site in Lincent, is considered as the excitation mechanism and is used to compute the axle loads $\hat{S}_{g_z kk}(\omega)$.

Figs. 20 and 21 compare the predicted and measured vibration velocity due to the passage of an IC-A and a Thalys train with a speed of 198 and 281 km/h, respectively. The agreement between both results is relatively good, which can also be explained by the more important contribution from axles close to the receiver points, which is predicted more accurately than the contribution from axles at a larger distance. The peak around 50 Hz in the experimental spectrum of the IC-A train is not found in the numerical results, however. As only the unevenness of the rail is accounted for in the simulation, this

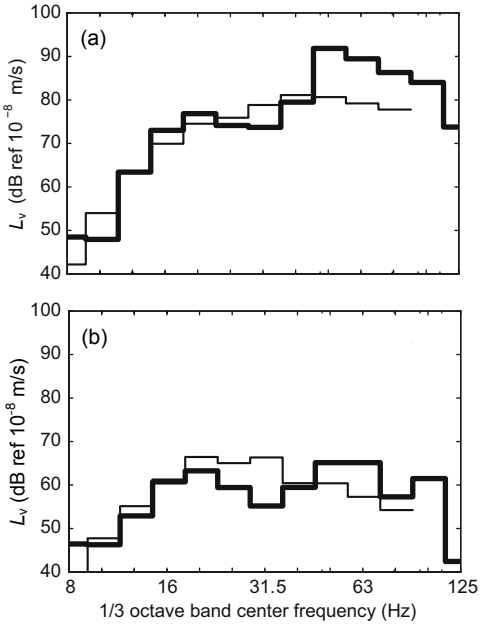

Fig. 20 Experimental (black line) and predicted (thin line) vibration velocity during the passage of an IC-A train at a speed of 198 km/h at (a) 6 m and (b) 24 m from the track

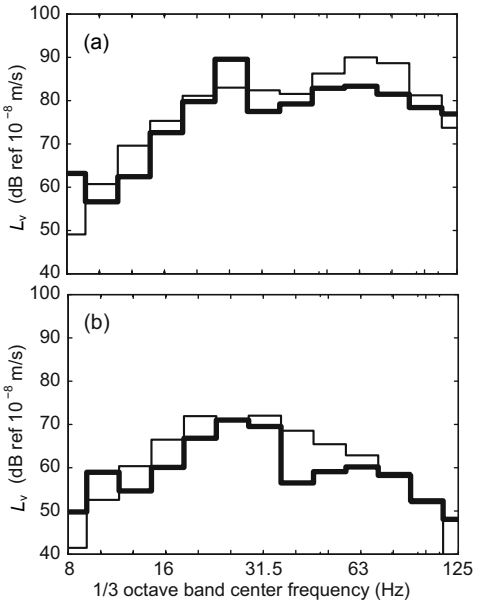

Fig. 21 Experimental (black line) and predicted (thin line) vibration velocity during the passage of a Thalys train at a speed of 281 km/h at (a) 6 m and (b) 24 m from the track

indicates that this peak is not caused by track or soil properties but by the dynamic vehicle characteristics or wheel unevenness. At larger distance, the peak in the experimental results is attenuated and the agreement is better. This second peak is not encountered in the spectrum for the Thalys train, and the prediction agrees relatively well with the experimental result.

5 Conclusions

In this paper, the measurement and the numerical prediction of transfer functions and ground vibration due to railway traffic is discussed.

First, the results from a measurement campaign at a site in Lincent (Belgium) next to the high-speed railway line between Brussels and Köln are discussed. The transfer functions between the track and the free field have been determined by means of a series of hammer impacts. The accuracy of the narrow band transfer functions is relatively good, especially for small source-receiver distances, and improves when represented in one-third octave bands.

Furthermore, the free field vibration velocity during several train passages of different types is measured. The results show a large variation of the vibration velocity level, especially close to the track, even for passages of the same train type. The variation is possibly due to variations of dynamic vehicle characteristics and wheel unevenness. A clear distinction can be made, however, between the average responses for different train types.

Second, a numerical model is presented that is based on the longitudinal invariance of the railway track. The model is used to predict the transfer functions and the vibration velocity due to a train passage. For the estimation of the vibration velocity level, a fixed position of the axle loads is assumed.

A discrepancy is observed between the predictions and the experimental results and shows the importance of accurate numerical models and input data. As input data for numerical predictions are often extracted from experimental results such as transfer functions, the problem is partially avoided by directly using experimental transfer functions in a prediction. A hybrid prediction technique is obtained by combining experimental transfer functions with predicted input data for the source and offers a possible solution for the lack of accuracy encountered in numerical predictions.

Acknowledgments

The first author is a PhD Fellow of the Research Foundation Flanders (FWO-Vlaanderen). The support of FWO is gratefully acknowledged.

References

Andersen, L., Jones, C.J.C., 2006. Coupled boundary and finite element analysis of vibration from railway tunnels–a comparison of two- and three-dimensional models. *Journal of Sound and Vibration*, **293**(3-5):611-625. [doi:10.1016/j.jsv.2005.08.044]

Coulier, P., Degrande, G., Dijckmans, A., Houbrechts, J., Lombaert, G., Rücker, W., Auersch, L., Rodríguez, M., Cuellar, V., Thompson, D., *et al.*, 2011. Scope of the Parametric Study on Mitigation Measures on the Transmission Path. RIVAS Deliverable D4.1.

Ewins, D.J., 1984. Modal Testing: Theory and Practise. Research Studies Press Ltd., Letchworth, UK.

François, S., Schevenels, M., Lombaert, G., Galvín, P., Degrande, G., 2010. A 2.5D coupled FE-BE methodology for the dynamic interaction between longitudinally invariant structures and a layered halfspace. *Computer Methods in Applied Mechanics and Engineering*, **199**(23-24):1536-1548. [doi: 10.1016/j.cma.2010.01.001]

Galvín, P., Dominguez, J., 2007. Analysis of ground motion

due to moving surface loads induced by high-speed trains. *Engineering Analysis with Boundary Elements*, **31**(11): 931-941. [doi:10.1016/j.enganabound.2007.03.003]

Hanson, C.E., Towers, D.A., Meister, L.D., 2005. High-Speed Ground Transportation Noise and Vibration Impact Assessment. HMMH Report 293630-4, US Department of Transportation, Federal Railroad Administration, Office of Railroad Development.

Hanson, C.E., Towers, D.A., Meister, L.D., 2006. Transit Noise and Vibration Impact Assessment. Report FTA-VA-90-1003-06, US Department of Transportation, Federal Transit Administration, Office of Planning and Environment.

Kogut, J., Degrande, G., 2003. Transfer Functions between the HST Track and the Free Field on the Line L2 Brussels-Köln in Lincent. Report BWM-2003-03, Department of Civil Engineering, KU Leuven, STWW Programme Technology and Economy, Project IWT-000152.

Lombaert, G., Degrande, G., Kogut, J., François, S., 2006. The experimental validation of a numerical model for the prediction of railway induced vibrations. *Journal of Sound and Vibration*, **297**(3-5):512-535. [doi:10.1016/j.jsv.2006.03.048]

Verbraken, H., Lombaert, G., Degrande, G., 2011. Verification of an empirical prediction method for railway induced vibrations by means of numerical simulations. *Journal of Sound and Vibration*, **330**(8):1692-1703. [doi:10.1016/j.jsv.2010.10.026]

Verbraken, H., Coulier, P., Lombaert, G., Degrande, G., 2012a. Measurement of Train Passages and Transfer Functions at a Site in Lincent. Report BWM-2012-05, Department of Civil Engineering, KU Leuven, Belgium.

Verbraken, H., Coulier, P., Lombaert, G., Degrande, G., 2012b. Measurement of Transfer Functions at a Site in Lincent. Report BWM-2012-07, Department of Civil Engineering, KU Leuven, Belgium.